Interplay between elastic interactions and kinetic processes in stepped Si (001) homoepitaxy

Wei Hong[1], Zhenyu Zhang[2, 3, 1] and Zhigang Suo[1]

[1]*Division of Engineering and Applied Sciences, Harvard University, Cambridge, MA 02138*

[2]*Materials Science and Technology Division, Oak Ridge National Laboratory, Oak Ridge, TN 37831*

[3]*Department of Physics and Astronomy, The University of Tennessee, Knoxville, TN 37996*

A vicinal Si (001) surface may form stripes of terraces, separated by monatomic-layer-high steps of two kinds, S_A and S_B. As adatoms diffuse on the terraces and attach to or detach from the steps, the steps move. In equilibrium, the steps are equally spaced due to elastic interaction. During deposition, however, S_A is less mobile than S_B. We model the interplay between the elastic and kinetic effects that drives step motion, and show that during homoepitaxy all the steps may move in a steady state, such that alternating terraces have time-independent, but unequal, widths. The ratio between the widths of neighboring terraces is tunable by the deposition flux and substrate temperature. We study the stability of the steady state mode of growth using both linear perturbation analysis and numerical simulations. We elucidate the delicate roles played by the standard Ehrlich-Schwoebel (ES) barriers and inverse ES barriers in influencing growth stability in the complex system containing (S_A+S_B) step pairs.

I Introduction

Because crystalline silicon is the foundation of many modern technologies, fundamental understanding of the energetics and atomic rate processes involved in Si homoexpitaxy constitutes an important area of basic research [1-22]. One primary objective of such studies is to gain precise control of the growth modes under various physically realistic conditions. Knowledge learned from this prototype model, in turn, may find applicability in other growth systems.

In this paper, we present a theoretical study of the interplay between elastic and kinetic effects on a surface vicinal to (001), tilted towards the [110] direction by a miscut angle (Fig. 1). We consider the case where the vicinal angle is sufficiently small, such that the surface consists of alternating terraces of two variants, T_A and T_B, and alternating monatomic-layer-high steps of two kinds, S_A and S_B [1, 9, 10]. The two variants of the terraces have identical atomic structures, except for a 90° rotation, with the dotted lines on each terrace in Fig. 1 representing dimer rows. The two kinds of steps, however, have dissimilar atomic structures [1]. During homoepitaxy, atoms from the gas phase deposit on the surface and diffuse on the terraces. As atoms attach to or detach from the steps, the steps move.

Several existing experimental observations motivated our model. During homoepitaxy, the S_B steps can catch up with the S_A steps to form bilayer steps [5]. Upon annealing, the bilayer steps split and relax to equally spaced monolayer steps [3, 9]. To account for the observation that S_A steps are less mobile than S_B steps, we require that adatoms on terraces overcome high energy barriers to attach to S_A steps, but low energy barriers to attach to S_B steps (Fig. 1). This requirement is also consistent with the experimental observation that, during a

certain period of annealing after rapid deposition, clusters near an S_B step disappear, but those near an S_A step remain [11]. These observations have led to a kinetic model [7, 13], in which different rates of attachment are assigned to the two kinds of steps, giving rise to the faster growth of the S_B steps. Formation of unequal width of the two variants of terraces can also be induced by electromigration, coupled with anisotropy in diffusivity [14], but in the present paper we exclude the consideration of the electromigration effect in our system.

The kinetic effect alone, however, cannot explain the equalization of the terrace widths during annealing. To account for the observations at annealing, following [2, 6], we invoke the anisotropic surface stress tensor. The anisotropy causes a discontinuity in the surface stress at each step (Fig. 1), an elastic field in the crystal, and repulsion between the neighboring steps. The elastic energy in the crystal minimizes when the monolayer steps are equally spaced.

We will include the above considerations in a model, and then use the model to study the motion of the steps. We will show that, at a finite deposition flux, the combined kinetic and elastic effects allow the steps to move in a steady state, such that alternating terraces have time-independent, but unequal, widths. The kinetic effect depends on the deposition flux and substrate temperature, while the elastic effect does not. By adjusting the deposition flux or temperature, one may obtain a vicinal surface with a desirable ratio between the widths of the alternating terraces. Such substrates possess different physical properties, for example tunable optical anisotropy [23], and may serve as useful templates for fabrication of functional materials on silicon.

II The elastic interactions between steps

As illustrated in Fig. 1, the steps are taken to be straight, with their positions at time *t* noted as $x_n^A(t)$ and $x_n^B(t)$. The coverage of adatoms on the terraces is a function of position and time, $c(x,t)$. The positions of the steps and the coverage of adatoms coevolve. In the absence of elastic interaction between the steps, the equilibrium coverage of adatoms on terraces is given by $c_0 = \exp(-E_0/kT)$, where E_0 is the formation energy of an adatom on terraces, *k* the Boltzmann constant and *T* the temperature in Kelvin.

We next describe how the elastic interactions between the steps modify the equilibrium coverage of adatoms. The surface stresses along and perpendicular to the direction of the dimer rows are different, noted as σ_A and σ_B, respectively (Fig. 1). Their difference, $\sigma_0 = \sigma_A - \sigma_B$, causes a discontinuity in the surface stress at every step, and an elastic field inside the crystal. Consequently, the elastic energy stored in the crystal changes when the steps move. The reduction in the elastic energy in the crystal associated with a step advance per unit area defines a thermodynamic driving force on the step, as given by [2, 24]

$$f_n^A = \sum_{m=\pm 1}^{\pm\infty} \frac{\alpha}{x_{n+m}^A - x_n^A} - \sum_{m=-\infty}^{+\infty} \frac{\alpha}{x_m^B - x_n^A} \text{ on step } x_n^A, \tag{1a}$$

and

$$f_n^B = \sum_{m=\pm 1}^{\pm\infty} \frac{\alpha}{x_{n+m}^B - x_n^B} - \sum_{m=-\infty}^{+\infty} \frac{\alpha}{x_m^A - x_n^B} \text{ on step } x_n^B, \tag{1b}$$

where

$$\alpha = \frac{\sigma_0^2}{2\pi} \frac{1-\nu}{\mu}, \tag{2}$$

with μ the shear modulus and ν Poisson's ratio. The sign of the discontinuity in the surface stress alternates from one step to another, so that the neighboring steps repel each other. By focusing on the forces of monopole nature shown in Eq. 1, we have neglected higher order effects (forces due to dipole and multipole coupling [10]), because we are interested in surfaces of small vicinal angles.

The above driving forces vanish when all the steps are equally spaced. When the steps are not equally spaced, however, the driving forces do not vanish, and the system is not in equilibrium. An adatom on a terrace may lower more energy by attaching to one step than the other. This effect is described as follows. Let Λ be the area per atomic site on the surface. When an adatom on a terrace attaches to step x_n^A, the step advances by area Λ, and the elastic energy of the crystal reduces by Λf_n^A. Consequently, the coverage of adatoms on the terrace in local equilibrium with the step x_n^A is

$$c_n^A = c_0 \exp\left(-\Lambda f_n^A / kT\right), \tag{3a}$$

A similar expression holds for the coverage of adatoms on terraces in local equilibrium with the step x_n^B:

$$c_n^B = c_0 \exp\left(-\Lambda f_n^B / kT\right). \tag{3b}$$

When the steps are not equally spaced, the driving forces f_n^A and f_n^B are nonzero. Consequently, the coverage of adatoms on terraces in local equilibrium with each step has a distinct value. This difference between the steps drives adatoms to preferentially attach to certain steps, leading to the changes in the widths of terraces.

III The growth kinetics

Assume that the system is in the step-flow regime. That is, the deposition flux F (i.e., fraction of a monolayer per unit time) is not high enough for islands to nucleate on the terraces. During homoepitaxy, atoms from the gas phase attach to the terraces as adatoms, which then diffuse to the steps. Once the adatoms attach to the steps, the steps move. The diffusivity of adatoms parallel to the dimer rows, D_B, is different from that perpendicular to the dimer rows, D_A (Fig. 1). The diffusion equation on a T_B terrace is written as

$$\frac{\partial c}{\partial t} = D_B \frac{\partial^2 c}{\partial x^2} + F \ . \tag{4}$$

At a low deposition flux, the motion of the steps is slow, so that we can assume the quasi-steady-state distribution of adatoms, i.e. $\partial c/\partial t = 0$. The resulting coverage profile on a T_B terrace is

$$c(x) = -\frac{F}{2D_B}\left(x - x_n^A\right)^2 + \beta_1^B\left(x - x_n^A\right) + \beta_0^B, \quad \left(x_n^A < x < x_n^B\right) \tag{5}$$

with the constants β_1^B and β_0^B set by the boundary conditions at the steps. Similarly, the coverage profile on a T_A terrace is

$$c(x) = -\frac{F}{2D_A}\left(x - x_{n-1}^B\right)^2 + \beta_1^A\left(x - x_{n-1}^B\right) + \beta_0^A, \quad \left(x_{n-1}^B < x < x_n^A\right), \tag{6}$$

As illustrated in Fig. 1, potential energy barriers exist for adatoms on terraces to attach to steps. These barriers are known as the Erlich-Schwoebel barriers [25] (ES, for adatoms from an upper terrace) and the inverse-ES barriers [20, 26] (iES, for adatoms from a lower terrace). Due to the iES barrier at the step x_n^A, the coverage of adatoms on the T_A terrace near the S_A step, $c\left(x_n^{A+}\right)$, differs from the equilibrium coverage of adatoms, c_n^A. Their difference, $c\left(x_n^{A+}\right) - c_n^A$, drives the attachment of adatoms to step x_n^A. Following Schwoebel [25], we adopt a linear

kinetic law, i.e. the number of atoms per length per unit time attaching to the step is given by $k_+^A\left[c\left(x_n^{A+}\right)-c_n^A\right]$, where k_+^A is the rate constant for adatoms to attach to the S_A step from the lower terrace, reflecting the existence of the iES barrier. Near the step x_n^A, the diffusion flux on the T_B terrace equals the rate at which adatoms attach to the step, namely,

$$J\left(x_n^{A+}\right)=-D_B\frac{\partial c}{\partial x}\Big|_{x_n^{A+}}=-k_+^A\left[c\left(x_n^{A+}\right)-c_n^A\right]. \tag{7}$$

Similarly, the diffusion flux on the T_A terrace equals the rate at which adatoms attach to the step x_n^A, namely,

$$J\left(x_n^{A-}\right)=-D_A\frac{\partial c}{\partial x}\Big|_{x_n^{A-}}=k_-^A\left[c\left(x_n^{A-}\right)-c_n^A\right], \tag{8}$$

where k_-^A is the rate constant for the adatoms to attach to the S_A step from the upper terrace, reflecting the existence of the ES barrier at the S_A step.

Both *ab initio* calculations [27, 28] and experimental observations [11] show that there is a low or even negative barrier on both sides of S_B steps. We therefore assume that, on both sides of an S_B step, the coverage of adatoms on the terraces is in local equilibrium, $c\left(x_n^B\right)=c_n^B$.

With these boundary conditions, the constants in (5) can be determined:

$$\beta_1^B=\frac{1}{D_B}\frac{\left(c_n^B-c_n^A\right)+\dfrac{F\left(l_n^B\right)^2}{2D_B}}{\dfrac{1}{k_+^A}+\dfrac{l_n^B}{D_B}},\quad \beta_0^B=\frac{c_n^A\dfrac{l_n^B}{D_B}+\dfrac{c_n^B}{k_+^A}+\dfrac{1}{k_+^A}\dfrac{F\left(l_n^B\right)^2}{2D_B}}{\dfrac{1}{k_+^A}+\dfrac{l_n^B}{D_B}}, \tag{9}$$

where $l_n^B=x_n^B-x_n^A$ is the width of the T_B terrace. Similarly, the constants in (6) are

$$\beta_1^A=\frac{1}{D_A}\frac{\left(c_n^A-c_{n-1}^B\right)+Fl_n^A\left(\dfrac{1}{k_-^A}+\dfrac{l_n^A}{2D_A}\right)}{\dfrac{1}{k_-^A}+\dfrac{l_n^A}{D_A}},\quad \beta_0^A=c_{n-1}^B. \tag{10}$$

where $l_n^A = x_n^A - x_{n-1}^B$ is the width of the T_A terrace.

The step x_n^A moves as adatoms on the terrace on either side attach to the step, namely

$$\frac{dx_n^A}{dt} = J\left(x_n^{A-}\right) - J\left(x_n^{A+}\right). \tag{11}$$

A similar equation holds for the step x_n^B. A combination of (5) – (11) leads to a set of ordinary differential equations that govern the motion of the steps:

$$\begin{cases} \dfrac{dx_n^A}{dt} = \dfrac{c_{n-1}^B - c_n^A + \dfrac{F\left(l_n^A\right)^2}{2D_A}}{\dfrac{1}{k_-^A} + \dfrac{l_n^A}{D_A}} + \dfrac{c_n^B - c_n^A + \dfrac{F\left(l_n^B\right)^2}{2D_B}}{\dfrac{1}{k_+^A} + \dfrac{l_n^B}{D_B}} \\ \dfrac{dx_n^B}{dt} = \dfrac{c_n^A - c_n^B + Fl_n^B\left(\dfrac{1}{k_+^A} + \dfrac{l_n^B}{2D_B}\right)}{\dfrac{1}{k_+^A} + \dfrac{l_n^B}{D_B}} + \dfrac{c_{n+1}^A - c_n^B + Fl_{n+1}^A\left(\dfrac{1}{k_-^A} + \dfrac{l_{n+1}^A}{2D_A}\right)}{\dfrac{1}{k_-^A} + \dfrac{l_{n+1}^A}{D_A}} \end{cases} \tag{12}$$

Given a set of initial conditions, $\left\{\cdots, x_{n-1}^A(0), x_{n-1}^B(0), x_n^A(0), x_n^B(0), x_{n+1}^A(0), x_{n+1}^B(0), \cdots\right\}$, we can evolve the positions of the steps by integrating (12).

IV Numerical simulations

We take representative parameters of the Si surface: the distance between two neighboring atoms along the [110] direction, $a = 3.84 \times 10^{-10}$ m; the area occupied by each atom on the (001) surface, $\Lambda = 1.47 \times 10^{-19}$ m^2; and the formation energy of an adatom, $E_0 \approx 1$eV [27, 28]. Taking a calculated value of the surface-stress anisotropy $\sigma_0 \approx 1\text{eV}/a^2 \approx 1$ N/m [6], and using the shear modulus $\mu = 80$ GPa and Poisson's ratio $\nu = 0.28$, we obtain that $\alpha \approx 10^{-12}$N. We represent diffusivities by $D_A = a^2\nu_0 \exp\left(-E_D^A/k_BT\right)$ and $D_B = a^2\nu_0 \exp\left(-E_D^B/k_BT\right)$, where the diffusion barriers are taken to be $E_D^A = 1\text{eV}$ and $E_D^B = 0.7\text{eV}$, with a jumping frequency ν_0 =

10^{13}Hz [4, 19, 29-32]. Different values of diffusion barriers have also been tried in the simulations, but such tests do not affect the qualitative behavior of the simulation results.

The magnitudes of the ES and iES barriers are less well established, and are left as fitting parameters in the present study. We prescribe the rate constants of attachment by $k_-^A = \frac{D_A}{a}\exp\left(-E_-^A/kT\right)$ and $k_+^A = \frac{D_B}{a}\exp\left(-E_+^A/kT\right)$, where E_-^A is the ES barrier and E_+^A is the iES barrier. They are additional barriers relative to the diffusion barriers E_D^A and E_D^B, respectively. For the time being we assume symmetric additional barriers, i.e. $E_-^A = E_+^A$. To "fit" the barrier height, we use the experimental observation that S_A does not move appreciably within 0.5 ML deposition [5]. In the simulations, we have tried three values: $E_\pm^A = 0.3$, 0.4 and 0.5eV. Following the experimental setup, we take the average terrace width to be 15nm, and the substrate temperature to be 750K. In the simulations, Si adatoms are deposited at a level of 1 ML/min for 1 minute, and then the system is relaxed at the same temperature, under which the steps recover an equal-spaced state in 10^3–10^4 minutes (Fig. 2). A total of 128 steps are simulated, with all other steps relocated by periodic boundary conditions. For the S_A steps to keep still during the deposition of the first half monolayer (a hard experimental fact to be reproduced [5], see more discussions on this point in Sec. VII), the additional barrier should be at least 0.4eV. The barrier height will also affect the relaxation time needed for the bilayer steps to split and recover to equally spaced monolayer steps. This relaxation time provides a possible method to experimentally determine the barrier height. At this writing, such experimental data are unavailable to us, and we will use an additional barrier of $E_\pm^A = 0.4\text{eV}$ in the remainder of the paper.

In our simulations, the algorithm does not allow the steps to overlap, and the increasing elastic repulsion between two steps very close to each other will maintain the small gap. A detailed study of the gap width and the step-step interaction may need higher-order elastic effects. For the time being, we will just regard such pairs as bilayer steps, without looking into the details in between.

Several simulated evolution sequences are shown in Figs. 3 and 4. Let L be the average width of the terraces, so that the average velocity of the steps is FL and, in time t, the average displacement of a step is FLt. The displacement of a step x relative to the average displacement is $(x - FLt)$. We plot the normalized relative displacements, $(x/L - Ft)$, for several steps as functions of time t. The initial conditions are that all the steps are equally spaced. As expected, at a finite deposition flux, the T_B terraces expand while the T_A terraces shrink. Such a change happens shortly after the deposition begins and takes less than a half monolayer of deposition to complete. Afterwards, a steady state is reached, in which both kinds of steps move at the same speed, and the ratio between the widths of the alternating terraces becomes constant. The step flow of unequally spaced steps, however, is often unstable. The steps bunch and form multilayer steps even at a relatively low deposition flux. This phenomenon has also been observed in experiments and explored theoretically [20, 33]. Nonetheless, both in simulations and in experiments, step bunching happens much slower than the redistribution of the two variants of the terraces. In simulations, step bunching takes place after a deposition of ~10 monolayers, while the change of the ratio between two variants of terraces completes in less than one monolayer of deposition.

A comparison between Figs. 3 and 4 shows that, at a higher substrate temperature, the transition from monolayer steps to bilayer steps happens at a higher deposition flux, and step bunching appears much later.

V Tunable ratio between the widths of the two variants of terraces

Now we consider the steady state, where every T_A terrace is of the same width l_A, and every T_B terrace is of another width l_B. The average terrace width is $L=\frac{1}{2}(l_A+l_B)$. In this case, all the S_A steps are equally spaced, so that the elastic driving force on every S_A step is the same, and results only from the presence of all the S_B steps:

$$f^A=-\sum_{n=-\infty}^{\infty}\frac{\alpha}{2nL-l_A}=\frac{\pi\alpha}{2L}\cot\frac{\pi l_A}{2L}. \tag{13}$$

Similarly, the elastic driving force on every S_B step is

$$f^B=-\frac{\pi\alpha}{2L}\cot\frac{\pi l_A}{2L}. \tag{14}$$

The equations of motion (12) reduce to

$$\begin{cases}\dfrac{dx_A}{dt}=\dfrac{-Q+\dfrac{Fl_A^2}{2D_A}}{\dfrac{1}{k_-^A}+\dfrac{l_A}{D_A}}+\dfrac{-Q+\dfrac{Fl_B^2}{2D_B}}{\dfrac{1}{k_+^A}+\dfrac{l_B}{D_B}}\\ \dfrac{dx_B}{dt}=\dfrac{Q+Fl_B\left(\dfrac{1}{k_+^A}+\dfrac{l_B}{2D_B}\right)}{\dfrac{1}{k_+^A}+\dfrac{l_B}{D_B}}+\dfrac{Q+Fl_A\left(\dfrac{1}{k_-^A}+\dfrac{l_A}{2D_A}\right)}{\dfrac{1}{k_-^A}+\dfrac{l_A}{D_A}}\end{cases} \tag{15}$$

with

$$Q=2c_0\sinh\left(-\frac{\pi\alpha\Lambda}{2kTL}\cot\frac{\pi l_A}{2L}\right). \tag{16}$$

In a steady state, the two kinds of steps have the same velocity $dx_A/dt = dx_B/dt$. A combination of (15) and (16) gives the equation that governs the steady state:

$$F = 4c_0 \sinh\left(-\frac{\pi\alpha\Lambda}{2kTL}\cot\frac{\pi l_A}{2L}\right)\frac{\frac{1}{k_-^A}+\frac{l_A}{D_A}+\frac{1}{k_+^A}+\frac{l_B}{D_B}}{\frac{2L}{k_-^A k_+^A}+l_A l_B\left(\frac{1}{k_-^A D_B}+\frac{1}{k_+^A D_A}\right)}. \quad (17)$$

Fig. 5 plots (17) at two temperatures. When the deposition flux is low, the two variants of terraces have a similar width, $l_A/L = 1$. When the deposition flux is high, the two variants of terraces have dissimilar widths, $l_A/L \to 0$. The transition occurs in a narrow range of deposition flux, and at higher deposition fluxes when the temperature is higher.

Such a transition, however, has so far not been reported experimentally. It is possible that the existing experiments were either at a too low temperature [17] or a too high deposition flux [5]. Under such conditions, bilayer steps and step bunching would always prevail over steady flow of monolayer steps. To obtain an intermediate ratio of the two variants of terraces at a vicinal angle of ~1°, our simulation suggests to deposit at a high temperature (>1000K), and a relatively low deposition flux (<0.01 ML per second). For surfaces of higher vicinal angles, however, the elastic interaction between steps is stronger, and the transition window will be at a higher flux or lower temperature.

VI Linear stability analysis

The motion of the monolayer steps has a translational symmetry, i.e., the velocity of a step is only a function of the positions of all other steps relative to it. The functional forms of the velocities in (16) are different for steps of the two different kinds, but are the same for all steps

of the same kind. This translational symmetry allows us to study the stability of the steady state by using the Fourier expansion.

In a steady state, all the steps move at the same speed, *FL*. To examine the stability of the steady state, we perturb the positions of both kinds of steps with the Fourier components of a single wavenumber *K*, namely,

$$\begin{cases} x_n^A = 2nL + FLt + \Delta^A \exp(iKn) \\ x_n^B = 2nL + l_B + FLt + \Delta^B \exp(iKn) \end{cases} \tag{18}$$

Note that even for one wavenumber *K*, the system of steps has two degrees of freedom, Δ^A and Δ^B, one for each kind of steps. Inserting (18) into (15), and retaining the terms linear in Δ^A and Δ^B, we obtain that

$$\frac{d}{dt}\begin{bmatrix} \Delta^A \\ \Delta^B \end{bmatrix} = \begin{bmatrix} \Omega_{11} & \Omega_{12} \\ \Omega_{21} & \Omega_{22} \end{bmatrix}\begin{bmatrix} \Delta^A \\ \Delta^B \end{bmatrix} \tag{19}$$

The coefficients Ω_{ij} are given by

$$\Omega_{11} = \frac{\frac{\xi}{4L}\left(P - S_- e^{-iK}\right) + F\frac{l_A}{D_A}}{\frac{1}{k_-^A} + \frac{l_A}{D_A}} + \frac{\xi\eta - Fl_A\frac{l_A}{2D_A}}{D_A\left(\frac{1}{k_-^A} + \frac{l_A}{D_A}\right)^2} + \frac{\frac{\xi}{4L}\left(P - S_-\right) - F\frac{l_B}{D_B}}{\frac{1}{k_+^A} + \frac{l_B}{D_B}} - \frac{\xi\eta - Fl_B\frac{l_B}{2D_B}}{D_B\left(\frac{1}{k_+^A} + \frac{l_B}{D_B}\right)^2}, \tag{20a}$$

$$\Omega_{12} = \frac{\frac{\xi}{4L}\left(S_+ - Pe^{-iK}\right) - Fe^{-iK}\frac{l_A}{D_A}}{\frac{1}{k_-^A} + \frac{l_A}{D_A}} - \frac{\xi\eta - Fl_A\frac{l_A}{2D_A}}{D_A\left(\frac{1}{k_-^A} + \frac{l_A}{D_A}\right)^2}e^{-iK} - \frac{\frac{\xi}{4L}\left(P - S_-\right) - F\frac{l_B}{D_B}}{\frac{1}{k_+^A} + \frac{l_B}{D_B}} + \frac{\xi\eta - Fl_B\frac{l_B}{2D_B}}{D_B\left(\frac{1}{k_+^A} + \frac{l_B}{D_B}\right)^2}, \tag{20b}$$

$$\Omega_{21} = \frac{\frac{\xi}{4L}\left(S_- - P\right)}{\frac{1}{k_+^A} + \frac{l_B}{D_B}} + F\left(e^{iK} - 1\right) + \frac{\xi\eta + Fl_B\left(\frac{1}{k_+^A} + \frac{l_B}{2D_B}\right)}{D_B\left(\frac{1}{k_+^A} + \frac{l_B}{D_B}\right)^2} - \frac{\frac{\xi}{4L}\left(Pe^{iK} - S_-\right)}{\frac{1}{k_-^A} + \frac{l_A}{D_A}} - \frac{\xi\eta + Fl_A\left(\frac{1}{k_-^A} + \frac{l_A}{2D_A}\right)}{D_B\left(\frac{1}{k_-^A} + \frac{l_A}{D_A}\right)^2}e^{iK}, \tag{20c}$$

$$\Omega_{22} = \frac{\frac{\xi}{4L}\left(P - S_+\right)}{\frac{1}{k_+^A} + \frac{l_B}{D_B}} - \frac{\xi\eta + Fl_B\left(\frac{1}{k_+^A} + \frac{l_B}{2D_B}\right)}{D_B\left(\frac{1}{k_+^A} + \frac{l_B}{D_B}\right)^2} + \frac{\frac{\xi}{4L}\left(P - S_+e^{iK}\right)}{\frac{1}{k_-^A} + \frac{l_A}{D_A}} + \frac{\xi\eta + Fl_A\left(\frac{1}{k_-^A} + \frac{l_A}{2D_A}\right)}{D_A\left(\frac{1}{k_-^A} + \frac{l_A}{D_A}\right)^2}, \tag{20d}$$

where $\xi = \frac{c_0 A\alpha}{k_B TL}$, $\eta = \pi \cot \frac{\pi l_B}{2L}$ and

$$\begin{cases} S_{\pm} = \sum_{m=-\infty}^{\infty} \frac{e^{imK}}{\left(m \pm \frac{l_B}{2L}\right)^2} \\ P = \pi K - \frac{K^2}{2} - \pi^2 \left(1 + \cot^2 \frac{\pi l_B}{2L}\right) \end{cases} \tag{21}$$

The 2×2 matrix $\boldsymbol{\Omega}$ has two eigenvalues. For the steady state to be stable, both eigenvalues should have negative real parts. Numerical calculations show that one of the eigenvalues always has a negative real part. Fig. 6 plots the real part of the other eigenvalue, $\mathrm{Re}\Omega_{\mathrm{MAX}}$, as a function of K, at the steady-states of various ratios of the widths of the alternating terraces, while the temperature is kept at 800K. In the plot, the growth rate is normalized by the deposition flux F. The almost-equally-spaced state (e.g., l_A/L = 0.9) is stable against perturbation of all wavenumbers. At low values of l_A/L, the step flow is unstable. However, even when the steps are nearly doubled (e.g., l_A/L = 0.1), the normalized growth rate is less than 0.8 (1/ML) in maximum. At such a rate, it will take at least 2~3 monolayers of deposition for an initial deviation ~1/10 of the terrace width to develop into a level comparable to the terrace width. By contrast, the tuning of the terrace coverage ratio is accomplished within a half monolayer of deposition.

VII Discussions

We have assumed that attachement barriers exist on both sides of the S_A step. This assumption is justified as follows. On a given terrace, say T_A, the rates at which adatoms attach to the S_A and S_B steps at the two ends should add up to the deposition flux. The ratio between the adatom fluxes attaching to the two steps depends on the additional barriers at the corresponding

steps. Because no or low additional barrier exists at the S_B step, the adatoms would have an equal probability of going to the S_A and S_B step if the barrier at the S_A step were also low. However, the experiment evidence [5] shows almost no attachment of adatoms on S_A step before doubling. Consequently, a relatively high additional ES barrier must exist at the S_A steps. A similar consideration of adatoms on a T_B terrace will conclude that an iES barrier exists at the S_A steps.

In a similar model proposed in [33], symmetric *absolute* barriers are assumed on both sides of the S_A steps. As the diffusion barrier on a T_A terrace is already high, such an assumption leads to almost no additional ES barrier. Consequently, the model fails to recover the experimental observations on a vicinal Si (001) surface. For example, a simulation in [33] shows that, instead of forming bilayer steps, both kinds of steps travel at almost the same speed, a prediction disagreeing with the experimental observation [5].

To determine the ES barrier at the S_A step, we have carried out another set of simulations, in which the iES barrier at the S_A step is taken to be 0.4eV while the ES barrier varies from 0.1eV to 0.4eV, and all other parameters are the same as in section IV. One monolayer of adatoms is deposited to the surface at a flux level of 1ML/min, followed by a full relaxation (of 10^4 minutes or longer) under the same temperature T = 750K. The results are shown in Fig. 7. In (a), when the ES barrier is taken to be 0.1eV (when the absolute barriers at S_A are symmetric), the S_B steps catch up with the next S_A step after almost one monolayer of deposition, during which the S_A steps have also moved by ¼ of the terrace width. Only when the ES barrier exceeds 0.4eV, the S_A step virtually keeps still before doubling. To recover the experimental evidence, we only need to have high enough barriers on both sides of the S_A step, but they do not

have to be the same. More simulations with asymmetric additional barriers have shown similar results.

In numerical simulation and linear stability analysis, we have found that the growth mode of steady-sate step flow is stable only under very small deposition flux, when the steps are almost equally spaced. This is in contradiction to the long recognized effect that the ES barriers stabilize step flow against step bunching [25, 34]. On a vicinal surface of a single kind of steps, a wider terrace, upon receiving more deposition, will transport more adatoms to attach to the upper step because of the ES barrier, so that the wider terrace will narrow down itself. On a vicinal Si (001) surface, however, this stabilizing effect of the ES barriers no longer operates. In a steady state, the combination of two neighboring terraces, T_B and T_A, can be regarded as a period of the structure, as illustrated in Fig. 1. The steady-state distance between two nearest S_A steps will be uniform along the surface. When a bi-terrace group gets wider and having more adatoms deposited, the direct result would be the faster motion of the S_B step in the middle, instead of a faster motion of the S_A step on the left. Consequently, in the presence of faster atomic sinks (the S_B steps), the ES barriers at S_A steps no longer stabilize the step flow. The only stabilizing mechanism is the elastic repulsion between the steps. This elastic effect, however, is overcome by the kinetic effect at high enough deposition flux.

The iES barriers at the S_A steps, on the other hand, are still effective. When an S_B step catches up with the next S_A step, the (S_B+S_A) pair effectively forms a bilayer step, with no ES barrier on the left, but a finite iES barrier on the right, inherited from the iES barrier of the S_A step. Just as in the case of vicinal surfaces with a single kind of steps, step flow is destabilized by the iES barriers [20]. On a wide terrace with more adatoms deposited, more diffusion flux

will be directed to the bilayer step on the right because of the presence of the iES; therefore, the bilayer step will move faster, making the wide terrace even wider.

VIII Concluding remarks

We have developed a model of step flow on vicinal Si (001) surfaces, taking into account both the elastic interaction between steps, and the dissimilar attachment kinetics at the two kinds of steps. Through steady-state analysis and numerical simulation, a continuous transition from equally spaced monolayer steps to bilayer steps has been predicted. Intermediate terrace coverage ratios can be obtained by tuning the deposition flux and the temperature. Consequently, it is possible to produce a vicinal Si surface with a tunable ratio of the alternating terraces.

The steady state of unequally spaced steps is unstable at high deposition fluxes. Step bunching is observed at finite deposition thickness, but later than the rearrangement of the terrace widths. The ES barrier, which stabilizes step flow against step bunching on a vicinal surface of single kind of steps, no longer stabilizes the step flow on vicinal Si (001) surfaces, because the S_B steps are more effective atomic sinks. The iES barrier, which destabilizes step flow and promotes step bunching, still operates effectively even on bilayer steps. The only stabilizing mechanism is the elastic repulsion between neighboring steps, which is effective at low deposition flux and high temperature.

Acknowledgements

This work was supported in part by Department of Energy Grant Nos. DEFG02-03ER46091 and DEFG02-05ER46209, and by Oak Ridge National Laboratory, managed by UTBattelle, LLC for the U.S. Department of Energy under DE-AC05-00OR22725.

References

[1] D. J. Chadi, Phys. Rev. Lett. **59**, 1691 (1987).

[2] O. L. Alerhand, D. Vanderbilt, R. D. Meade and J. D. Joannopoulos, Phys. Rev. Lett. **61**, 1973 (1988).

[3] K. Sakamoto, T. Sakamoto, S. Nagao, G. Hashiguchi, K. Kuniyoshi, and N. Taskahashi, in Proceedings of the Second International Symposium on Silicon Molecular Beam Epitaxy, Honolulu, Hawaii, 1987, edited by J. C. Bean and L. J. Schowalter (Electrochemical Society, Pennington, NJ, 1988).

[4] Y.-W. Mo, B. S. Swartzentruber, R. Kariotis, M. B. Webb, and M. G. Lagally, Phys. Rev. Lett. **63**, 2393 (1989).

[5] A. J. Hoeven, J. M. Lenssinck, D. Dijkkamp, E. J. van Loenen, and J. Dieleman, Phys. Rev. Lett. **63**, 1830 (1989).

[6] O. L. Alerhand, A. N. Berker, J. D. Joannopoulos, D. Vanderbilt, R. J. Hamers, and J. E. Demuth, Phys. Rev. Lett. **64**, 2406 (1990).

[7] S. Stoyanov, Europhys. Lett. **11**, 361 (1990).

[8] T. W. Poon, S. Yip, P. S. Ho, and F. F. Abraham, Phys. Rev. Lett. **65**, 2161 (1990).

[9] X. Tong and P. A. Bennett, Phys. Rev. Lett. **67**, 101 (1991).

[10] E. Pehlke and J. Tersoff, Phys. Rev. Lett. **67**, 465 (1991).

[11] Y.-W. Mo and M. G. Lagally, Surf. Sci. **248**, 313 (1991).

[12] Z. Y. Zhang, Y.-T. Lu, and H. Metiu, Phys. Rev. B. **46**, 1917 (1992).

[13] S. Stoyanov, App. Surf. Sci. **60**, 55 (1992).

[14] S. Stoyanov, M. Ichikawa and T. Doi, Jpn. J. Appl. Phys. **32**, 2047 (1993).

[15] Z. Y. Zhang, F. Wu, and M. G. Lagally, Annu. Rev. Mater. Sci. **27**, 525 (1997).

[16] J. van Wingerden, A. van Dam, M. J. Haye, P. M. L. O. Scholte, and F. Tuinstra, Phys. Rev. B. **55**, 9352 (1997).

[17] C. Schelling, G. Springholz, and F. Schäffler, Phys. Rev. Lett. **83**, 995 (1999).

[18] J. Nara, T. Sasaki, T. Ohno, J. Cryst. Growth **201**/**202**, 77 (1999).

[19] J. Zi, B. J. Min, Y. Lu, C. Z. Wang, and K. M. Ho, App. Phys. Lett. **77**, 4184 (2000)

[20] J. Mysliveček, C. Schelling, F. Schäffler, G. Springholz, P. Šmilauer, J. Krug, and B. Voigtländer, Surf. Sci. **520**, 193-206 (2002).

[21] C. Teichert, Phys. Rep. **365**, 335 (2002).

[22] C. V. Ciobanu, D. T. Tambe, V. B. Shenoy, C.-Z. Wang and K.-M. Ho, Phys. Rev. B **68**, 201302(R) (2003).

[23] S. G. Jaloviar, J.-L. Lin, F. Liu, V. Zielasek, L. McCaughan, and M. G. Lagally, Phys. Rev. Lett. **82**, 791 (1999).

[24] V. I. Marchenko, A. Y. Parshin, Zhurnal Eksperimentalnoi I Teoreticheskoi Fiziki **79**, 257 (1980).

[25] R. L. Schwoebel, J. Appl. Phys. **40**, 614 (1969); G. Ehrlich and F. G. Hudda, J. Chem. Phys. **44**, 1039 (1966); R. L. Schwoebel and E. J. Shipsey, J. Appl. Phys. **37**, 3682 (1966).

[26] J. Krug, V. Tonchev, S. Stoyanov and A. Pimpinelli, Phys. Rev. B **71**, 045412 (2005).

[27] Q.-M. Zhang, C. Roland, P. Boguslawski, and J. Bernholc, Phys. Rev. Lett. **75**, 101 (1995)

[28] S. Jeong, A. Oshiyama, Surf. Sci. **433-435**, 481 (1999).

[29] Z. Y. Zhang, F. Wu, H. J. W. Zandvliet, B. Polesema, H. Metiu, and M. G. Lagally, Phys. Rev. Lett. **74**, 3644 (1995).

[30] B. S. Swartzentruber, Phys. Rev. Lett. **76**, 459 (1996).

[31] B. Borovsky, M. Krueger, and E. Ganz, Phys. Rev. Lett. 78, 4229 (1997).

[32] G. M. Dalpian, A. J. R. da Silva, and A. Fazzio, Phys. Rev. B. 70, 193306 (2004).

[33] T. Frisch and A. Verga, Phys. Rev. Lett. **94**, 226102 (2005).

[34] W. Hong, H. N. Lee, M. Yoon, H. M. Christen, D. H. Lowndes, Z. Suo, and Z. Zhang, Phys. Rev. Lett. **95**, 095501 (2005).

Figures

Figure 1 (a) A schematic of the Si (001) vicinal surface, tilted towards the [110] direction by a small angle. The dotted lines on the terraces are the directions of dimer rows. (b) A schematic of the energy landscape for an adatom on the surface. Attachement barriers exist on both sides of the S_A steps, but no attachement barriers exist around the S_B steps. On terraces, adatoms diffuse faster along the dimer row direction than perpendicular. (c) The discontinuity in the surface stress at every step.

Figure 2 Simulation of deposition at 1ML/min for 1 minute, followed by relaxation. The substrate temperature is kept at 750K. The additional ES and iES barriers at the S_A step are set to be (a) 0.3eV (b) 0.4eV (c) 0.5eV.

Figure 3 The simulated motion of steps at temperature T = 800K and four levels of the deposition flux. When the deposition flux is low, step flow persists stability. When the deposition flux is high, the two kinds of terraces quickly adjust to unequal widths, but then step bunching sets in.

Figure 4 The simulated step growth processes at temperature T = 1000K and four levels of deposition flux. The trend is similar as that at T = 800K (Fig. 3), but step bunching sets in at a higher deposition flux at T = 1000K than at T = 800K.

Figure 5 Transition from monolayer steps to bilayer steps. When l_A/L = 1, the steps are equally spaced. When l_A/L = 0, bilayer steps form. The transition occurs at higher fluxes at a higher temperature.

Figure 6 Growth rate of the faster eigenmode as a function of the wavenumber K. The growth rate is normalized with the deposition flux, so that the vertical scale is in units of (1/monolayer). The steady state is more unstable at higher deposition flux or lower l_A/L.

Figure 7 Simulation of deposition at 1ML/min for 1 minute followed by relaxation. The temperature is kept at a constant value of 750K. The ES barrier at the S_A steps is set to (a) 0.1eV, (b) 0.2eV, and (c) 0.4eV, while the iES barrier is fixed at 0.4eV.

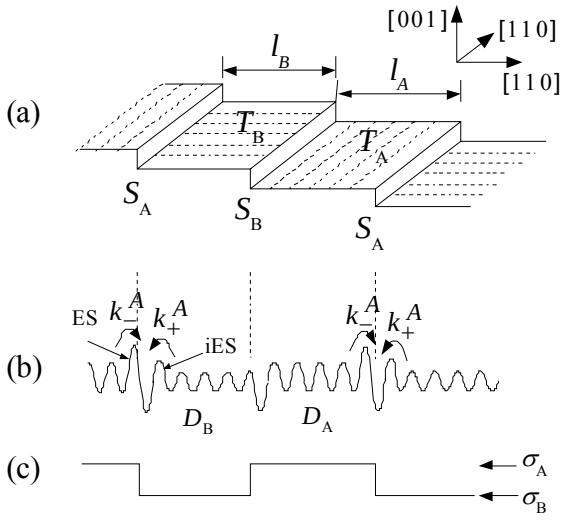

Fig. 1 (Hong, Zhang, & Suo)

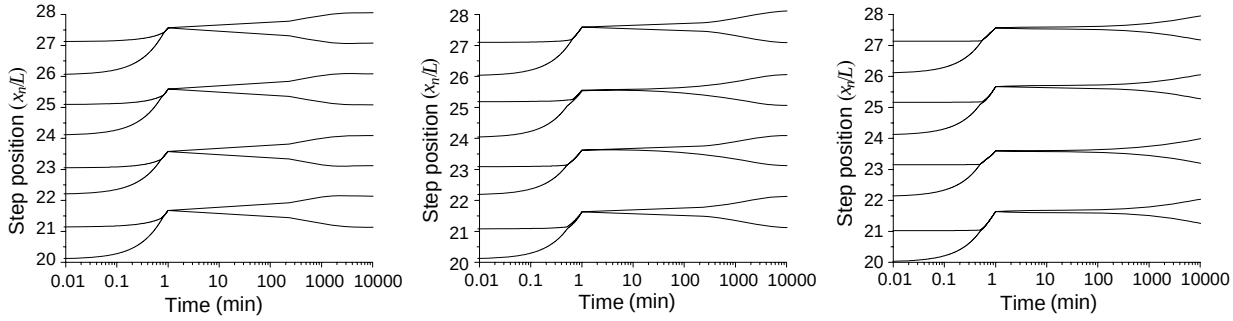

(a) (b) (c)

Fig. 2 (Hong, Zhang, & Suo)

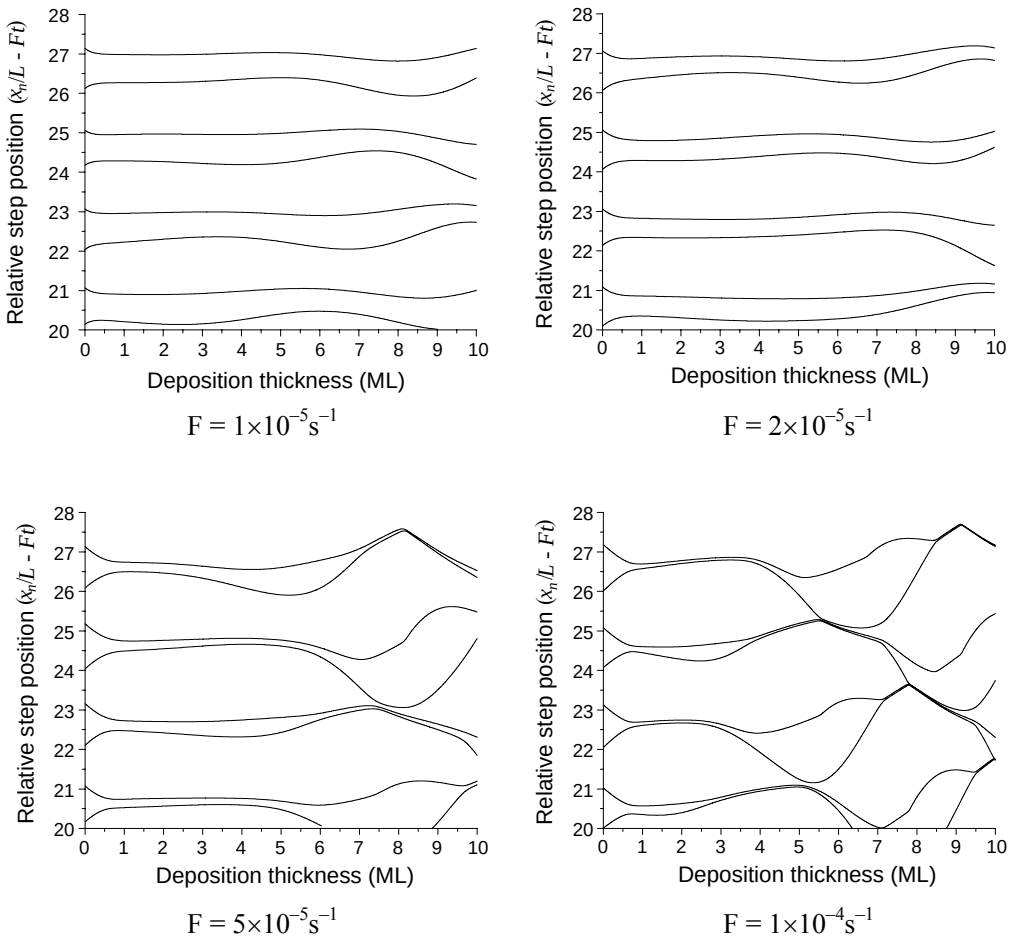

Fig. 3 (Hong, Zhang, & Suo)

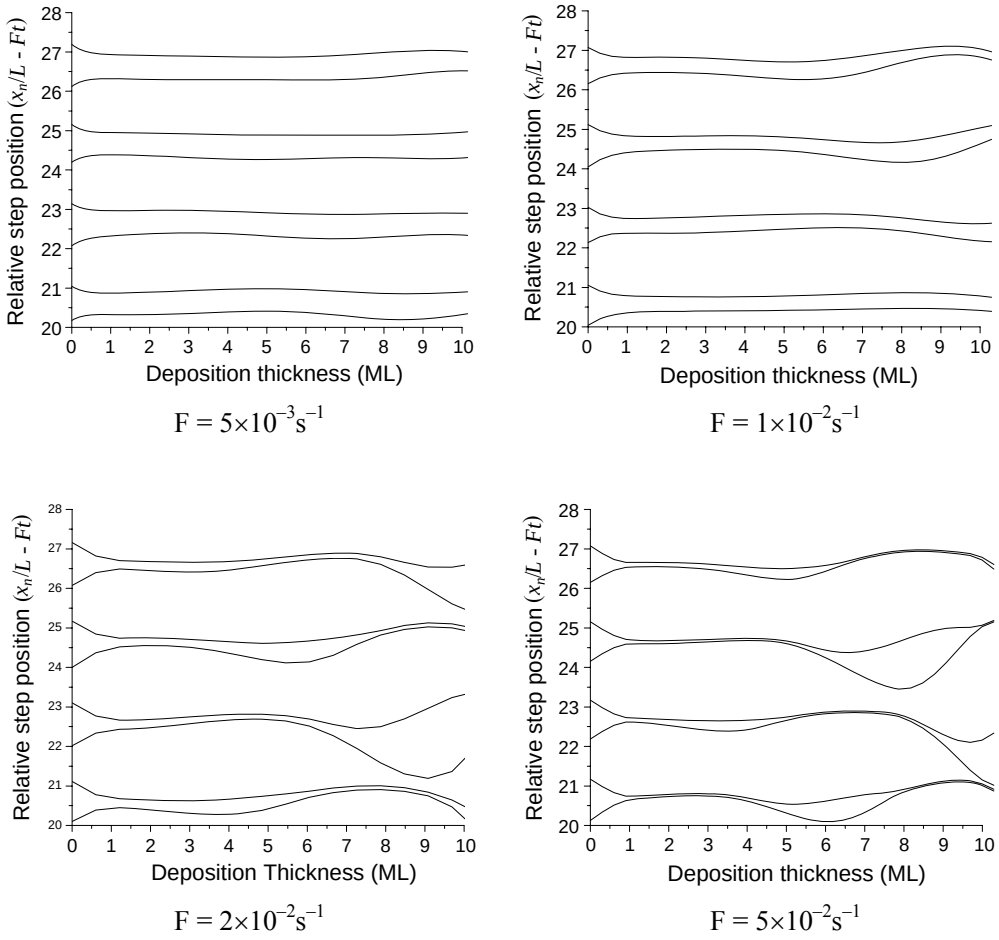

Fig. 4 (Hong, Zhang, & Suo)

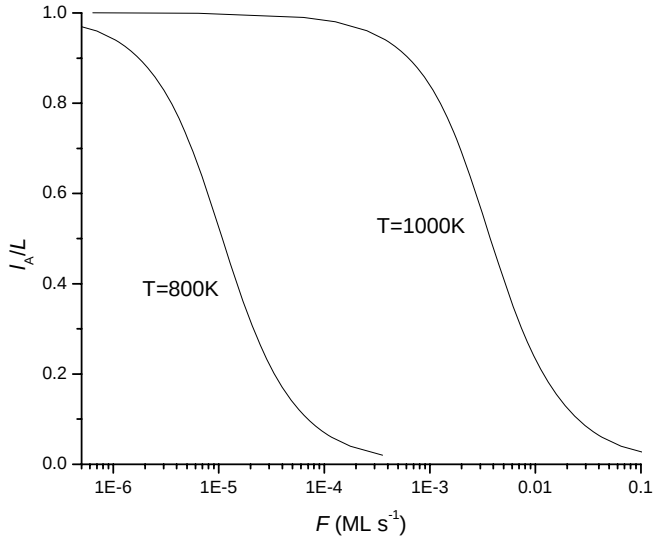

Fig. 5 (Hong, Zhang, & Suo)

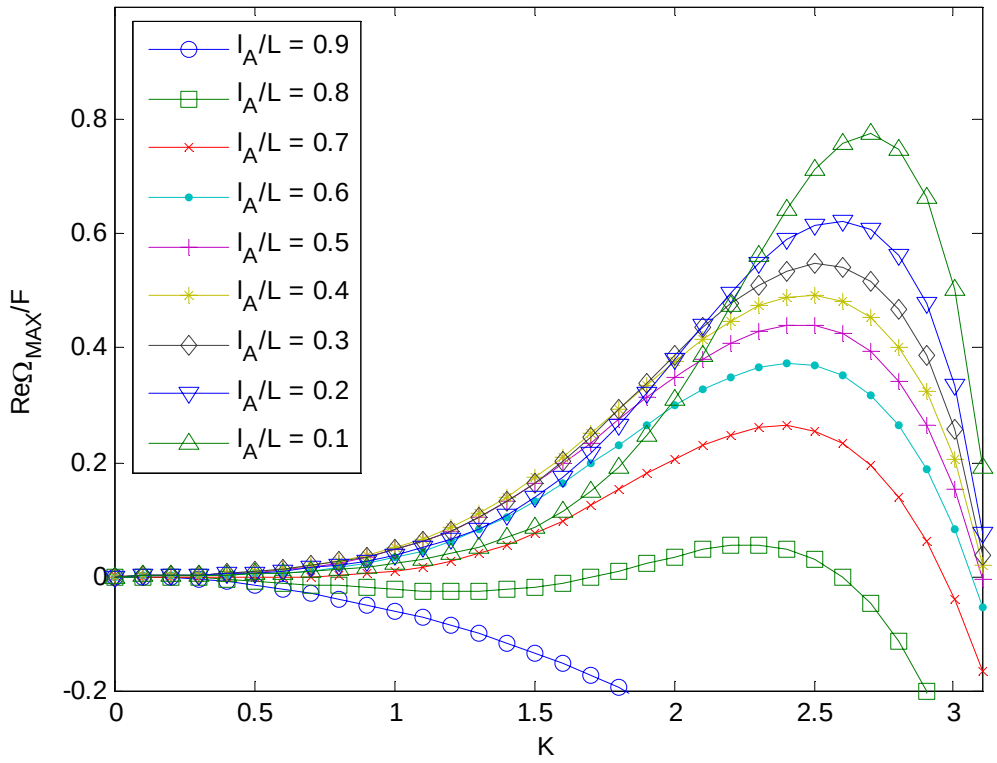

Fig. 6 (Hong, Zhang, & Suo)

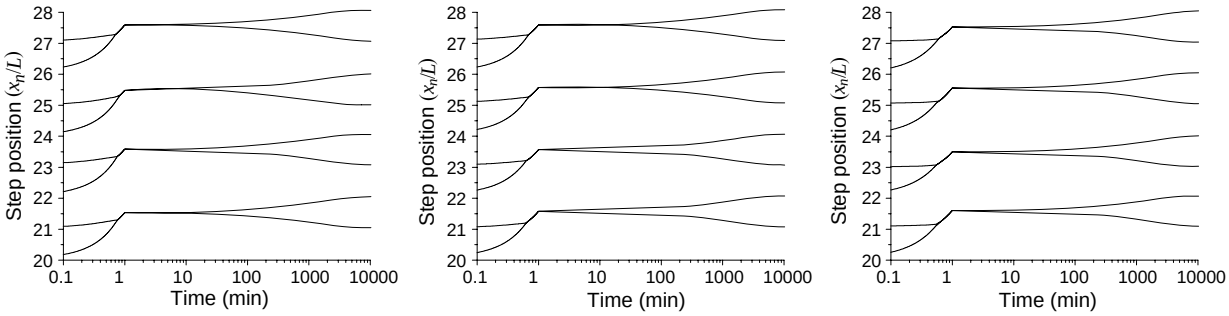

(a) (b) (c)

Fig. 7 (Hong, Zhang, & Suo)